Seasonal variations and controlling factors of nitrogen fluxes at the sediment-water interface in a semi-enclosed inland sea

Zhaosen Wu[1, 2], Xinyu Guo[2, *], Jie Shi[1, 3], Xiaokun Ding[4], Masatoshi Nakakuni[5, 6], Kuninao Tada[5, 6]

[1]Key Laboratory of Marine Environment and Ecology, Ministry of Education of China, Ocean University of China, 238 Songling Road, Qingdao 266100, China

[2]Center for Marine Environmental Studies, Ehime University, 2-5 Bunkyo-Cho, Matsuyama 790-8577, Japan

[3]Laboratory for Marine Ecology and Environmental Sciences, Qingdao National Laboratory for Marine Science and Technology, Qingdao, 266071, China

[4]School of Ocean, Yantai University, Yantai, 264005, China

[5]Faculty of Agriculture, Kagawa University, Ikenobe, Kita, Miki, Kagawa 761-0701, Japan

[6]Seto Inland Sea Regional Research Center, Kagawa University, Saiwai, Takamatsu, Kagawa 761-0016, Japan

Corresponding to: Xinyu Guo (guo.xinyu.mz@ehime-u.ac.jp) ORCID: 0000-0002-4832-8625

Abstract. Nitrogen fluxes across the sediment-water interface and nitrogen removal from sediments are essential components of the nitrogen cycle and ecosystem in semi-enclosed inland seas. However, the difficulty in observational sampling hinders the acquisition of continuous data necessary to understand their seasonal variations and underlying mechanisms. In response to this issue, we have developed a one-dimensional vertical model of the nitrogen cycle within sediments and used it to reproduce the seasonal changes of observed nitrogen fluxes in a typical semi-enclosed inland sea and investigate their controlling factors through sensitivity experiments. Model results indicate that 48% of particulate organic nitrogen (PON) settling into sediments is returned to the bottom water as dissolved inorganic nitrogen (DIN), while 6% is removed via N-loss flux (dinitrogen gas and nitrous oxide). The seasonal variations of PON and DIN fluxes are governed by fundamentally different environmental factors, highlighting the necessity of accounting for seasonal changes in bottom-water temperature and nitrogen concentrations when estimating DIN flux in the sediment–water interface. Nitrogen removal is dominated by denitrification. However, its overall magnitude remains relatively low, constrained by the oligotrophic conditions in our study site.

Keywords: sediment-water interface, semi-enclosed inland sea, nitrogen fluxes, sediment model, nitrogen removal

1 Introduction

Sediments play a crucial role in regulating the storage and removal of nitrogen within semi-enclosed inland seas, which significantly influences the balance and stability of the ecosystem (Huettel et al., 2014; Zhang et al., 2020; Kalvelage et al., 2013; Thamdrup, 2012). On one hand, the sediment can bury substantial amounts of nitrogen, potentially on par with river inputs (Liu et al., 2021; Han et al., 2021; Lønborg and Markager, 2021). On the other hand, because of remineralization, the sediment continuously releases dissolved inorganic nitrogen (DIN) into the overlying water (Devol, 2015; Boynton et al., 2017; Liu et al., 2012). In the semi-enclosed inland sea, vertical mixing facilitates the contribution of DIN from sediments as a vital nutrient source for primary production because of shallow water depth (Huettel et al., 2014; Yi et al., 2023; Leng et al., 2023; Liu and Yin, 2007; Berelson et al., 2013; Leynaert et al., 2011; Mei Liu et al., 2011). Notably, the sediment serves as the primary anoxic environment in these regions, where key nitrogen removal processes, such as denitrification and anammox, occur. These processes are essential for regulating nitrogen inventories and influencing nutrient structure in these areas. Researches indicate that continental shelves, which constitute merely 7.5% of the global seafloor, are responsible for 44% of fixed nitrogen losses (Devol, 2015; Mctigue et al., 2016; Huang et al., 2021; Jäntti and Hietanen, 2012; Khalil and Rasmussen, 2012). Furthermore, nitrous oxide, a byproduct of denitrification, is a significant greenhouse gas that contributes to global warming (Wilson et al., 2020; Yang et al., 2022).

To clarify the function of the sediment in ecological and environmental changes, it is necessary to conduct a quantitative analysis of nitrogen fluxes at the sediment-water interface in semi-enclosed inland seas, along with their seasonal variations. Direct observation of particulate organic nitrogen (PON) flux at this interface poses challenges due to the influence of resuspension processes. Consequently, numerous studies focused on DIN flux and its seasonal variations primarily through in situ observations, incubation experiments, or estimations based on Fick's law (De Vittor et al., 2012; Mu et al., 2017; Chen et al., 2023). For example, studies in the northern Adriatic Sea and the Baltic Sea have demonstrated the same conclusion that DIN flux exhibits seasonal variations, with higher levels in summer and lower levels in winter, likely influenced by water temperature (De Vittor et al., 2012; Niemistö et al., 2018). The fluxes of dinitrogen gas and nitrous oxide are mainly accessed through the measurement of denitrification and anammox rates within sediments (Zhang et al., 2018; Rich et al., 2020). A study conducted in the Pearl

River Estuary reported that the denitrification rate in sediments also displayed seasonal variability, with peak values observed in summer and reduced values in winter (Teng and Lin, 2024). However, the challenges and cost associated with field sampling limit the feasibility of continuous monitoring of these fluxes. Moreover, the direction of DIN flux varies across different regions, with the underlying mechanisms remaining unclear (Mu et al., 2017; De Vittor et al., 2015; Dale et al., 2022; Bohlen et al., 2011; Ratmaya et al., 2022; Zhou et al., 2022). Therefore, identifying the magnitude and direction of nitrogen fluxes at the sediment-water interface in semi-enclosed inland seas, along with their seasonal patterns and underlying controlling mechanisms, is crucial for understanding the contribution of sediments to the aquatic ecosystem in these regions.

Numerical modelling is a valuable tool for understanding the factors that govern nitrogen fluxes at the sediment-water interface. Typically, nitrogen fluxes at this interface derived from empirical formulas serve as essential boundary conditions for modelling the aquatic nitrogen cycle in semi-enclosed inland seas (Lønborg and Markager, 2021). However, this approach largely overlooks the changes occurring within the sediment and the corresponding flux responses to these alterations. An alternative approach is the implementation of a box model, which investigates nitrogen processes within the sediment. Nonetheless, the box model's treatment of all sediment as a single domain, coupled with its failure to account for the vertical distribution of chemical substances—particularly oxidants such as dissolved oxygen (DO)—limits its capacity to provide a comprehensive understanding of the nitrogen cycling processes within the sediment (Yang et al., 2022). A one-dimensional vertical sediment model addresses this limitation, albeit at the cost of increased complexity and computational demands. This model has demonstrated efficacy in accurately reproducing seasonal variations in nitrogen fluxes at the sediment-water interface (Radtke et al., 2019; Umlauf et al., 2023). Despite the clear advantages of this model|ing approach over empirical formulas and box models, well-validated applications remain relatively scarce.

This study focuses on the unclear seasonal variations in the magnitude and direction of nitrogen fluxes at the sediment–water interface in semi-enclosed inland seas, alongside the insufficiently understood underlying mechanisms with controlling factors driving these changes. We developed a one-dimensional vertical sediment model to simulate nitrogen cycling and accurately quantify nitrogen fluxes at the interface. Supported by monthly continuous observations conducted in the bottom water and sediment of Harima Nada in Japan, a typical semi-enclosed inland sea, we obtained a robust dataset for model

validation. The model successfully reproduced the seasonal variations in the concentrations of three nitrogen species within the sediment and nitrogen fluxes at the sediment-water interface. Additionally, numerical experiments further elucidated the influence of key environmental factors on these seasonal variations. This study aspires to establish a scientific foundation for comprehending the role of sediment nitrogen cycling in influencing the ecological environment of semi-enclosed marine systems. The findings can provide crucial support for offshore environmental remediation and the development of management policies.

2 Materials and Methods

2.1 Study area

Harima Nada is situated within Seto Inland Sea, the largest semi-enclosed sea in Japan (Figure 1). It has an average water depth of 26 meters and is connected to Osaka Bay and Hiuchi Nada on the eastern and western sides, respectively. To the south, it connects to the Pacific Ocean through the Naruto Strait and Kii Channel (Zhu et al., 2019; Chang et al., 2009). Harima Nada is strongly controlled by seasonal variations in wind forcing and density structure (Tong-u-dom et al., 2023). Its hydrographic circulation exhibits clear seasonal patterns: in winter, a wind-driven downwind circulation dominates under the prevailing north-westerly winds, whereas in summer, a density-driven cyclonic circulation develops due to the horizontal change in stratification. The water column structure also shows pronounced seasonality. Stratification intensifies in summer, promoting the formation of bottom cold water, while in winter, the water column becomes vertically well mixed. These seasonal changes in circulation and stratification jointly regulate the spatial distribution of temperature, salinity, and currents within the basin.

Based on the dataset from the Japanese Ministry of the Environment (https://water-pub.env.go.jp/water-pub/mizu-site/mizu/kouiki/dataMap.asp), DO concentrations in Harima Nada range from 6 to 10 mg L^{-1} (Figure S1). Surface DO exhibits clear seasonal variability, with the lowest values observed in autumn and the highest in winter. Controlled by hydrodynamic conditions, bottom DO reach its minimum in summer due to the intensification of stratification, while vertical mixing in winter leads to the highest bottom DO concentrations.

Chlorophyll concentrations and primary production in the water column are primarily regulated by nutrient availability (Leng et al., 2023; Tong-u-dom et al., 2025). During summer, elevated chlorophyll levels are observed in the estuarine region due to increased riverine nutrient input (Figure S2). In autumn and winter, enhanced vertical mixing redistributes DO, promoting higher chlorophyll concentrations in bottom waters. Previous study has estimated the annual primary production in Harima Nada to be approximately 41 g N m^{-2} yr^{-1} (Tada, 2021). As moving to the sea bottom, most of the sediments in the Harima Nada are muddy, with a mud content exceeding 70%.

Over the past several decades, the environment of the Seto Inland Sea has undergone significant changes (Ishii et al., 2014; Yamamoto et al., 2021). With the continuous observations of sediments in Harima Nada by our collaborators, we have realized that the DIN input from sediments in this area is comparable to that from rivers, exhibiting notable seasonal variations (Leng et al., 2023; Nakakuni et al., 2024). However, the driving factors and mechanisms behind these seasonal changes remain unclear. Therefore, Harima Nada serves as an excellent study area, and these observational data can provide a sufficient validation to ensure the reliability of model results (Nakakuni et al., 2024). This allows us to examine the seasonal variations in sediment nitrogen cycling and interfacial nitrogen fluxes, as well as their controlling mechanisms. Additionally, this study lays the groundwork for future exploration of how sediment nitrogen cycling responds to long-term changes in the aquatic environment.

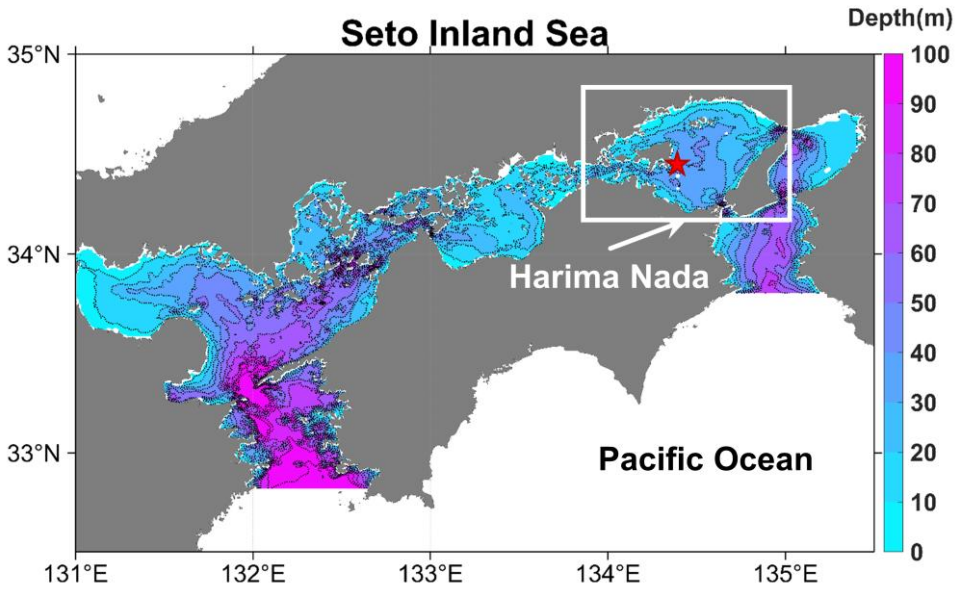

Figure 1. Study area of the Harima Nada, Japan. The red star represents the site where the observational data used in this study were collected.

2.2 Model descriptions

Based on the theory of early diagenesis (Berner, 1980), we have developed a biogeochemical model for sediment (Figure 2). This model encompasses two components: solid matter and pore water. The state variables consist of the concentrations of two types of PON (fast-decayed and slow-decayed ones) for the solid matter and the concentrations of NH_4^+, NO_2^-, NO_3^-, DO and ODU (the oxygen demand units) in the pore water. Additionally, we set a fluff layer at the top of sediment, where the active benthos and material exchange processes with the above water column occur (Lee et al., 2002; Kuhrts et al., 2006; Laima et al., 2002).

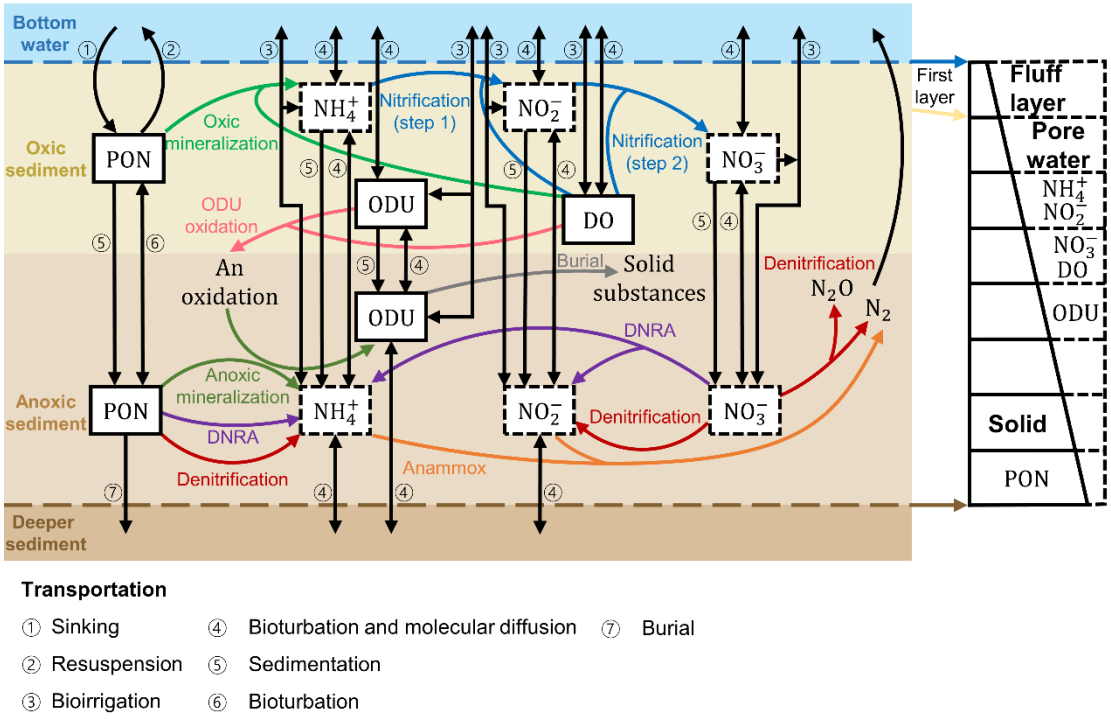

Figure 2. Physical and biogeochemical processes for nitrogen cycle in the sediment model. Six state variables in the model are PON, $\mathbf{NH_4^+}$, $\mathbf{NO_2^-}$, $\mathbf{NO_3^-}$, DO and ODU (the oxygen demand units). PON is a solid substance (enclosed by solid lines), while $\mathbf{NH_4^+}$, $\mathbf{NO_2^-}$, $\mathbf{NO_3^-}$, DO and ODU are dissolved substances in the pore water (enclosed by dash lines). The physical processes and biogeochemical processes are denoted by black arrows and coloured arrows, respectively. The numbers with circle denote the transport processes included in the model.

In the solid part, the fast-decayed and slow-decayed PON are treated with a large and small mineralization rate, respectively. Both of them undergo identical vertical transport processes, including downward sedimentation driven by gravity and vertical diffusion caused by bioturbation. Their mineralization occurring within the sediment provides a flux of NH_4^+ into the pore water.

In the pore water, the dissolved NH_4^+, NO_2^-, NO_3^-, DO and ODU are transported downward and diffused vertically, as corresponding to both bioturbation and molecular diffusion. The biogeochemical processes occurring within the pore water include nitrification, denitrification, anammox, dissimilatory nitrate reduction to ammonium (DNRA), ODU oxidation and ODU burial.

At the sediment-water interface, the exchange of solid matter is controlled by the bottom shear stress. The solid matter in the water column sinks into the fluff layer when the bottom stress is below a critical value, while resuspension occurs when the bottom stress exceeds this threshold. The exchange fluxes of NH_4^+, NO_2^-, NO_3^-, DO and ODU at the interface are determined by the product of the diffusion coefficient and their concentration gradient between the fluff layer and the overlying water.

In the deepest layer of sediment, only the slow-decayed PON is allowed to move downward and leave the model domain via burial. The exchange fluxes of NH_4^+, NO_2^- and ODU between the model domain and the underlying pore water are calculated by the production of the diffusion coefficient and the concentration gradient derived from the model results at the nearest grid point and the observations in the underlying pore water, while the exchange fluxes of NO_3^- and DO there are set to zero.

2.3 Equations and parameters

The equations for the concentrations of solid matter ($C_s, \mathrm{mmol\ m^{-3}}$) and dissolved matter ($C_d, \mathrm{mmol\ m^{-3}}$) are as follows:

$$\frac{\partial[(1-\emptyset)\cdot C_s]}{\partial t} = \frac{\partial[(1-\emptyset)\cdot D_B\cdot\frac{\partial C_s}{\partial z}]}{\partial z} - \frac{\partial[\omega\cdot(1-\emptyset)\cdot C_s]}{\partial z} + (1-\emptyset)\cdot\sum R_s \quad (1)$$

$$\frac{\partial[\emptyset\cdot C_d]}{\partial t} = \frac{\partial[\emptyset\cdot(D_B+D_M)\cdot\frac{\partial C_d}{\partial z}]}{\partial z} - \frac{\partial[\omega\cdot\emptyset\cdot C_d]}{\partial z} + \emptyset\cdot\alpha\cdot(C_d^w - C_d) + \emptyset\cdot\sum R_d \quad (2)$$

Where z (m) is vertical axis for sediment depth, t (s) is time, $\emptyset$ is the sediment porosity, D_B ($m^2\ s^{-1}$) is the bioturbation coefficient , D_M ($m^2\ s^{-1}$) is the molecular diffusion coefficient, ω ($m\ s^{-1}$) is the sedimentation velocity, α (s^{-1}) is the bioirrigation coefficient, C_d^w ($mmol\ m^{-3}$) is the concentration of dissolved matter in the bottom water, R_s is the biochemical reaction rate of PON, and R_d is the biochemical reaction rate of dissolved matter, including NH_4^+, NO_2^-, NO_3^-, DO and ODU. Since the sediment type in the study area is muddy, the advection of pore water in sandy sediments controlled by pressure is neglected.

The vertical profile of D_B is expressed as equation (3) (Radtke et al., 2019).

$$D_B(z) = \begin{cases} D_{B_{max}}, & 0 < z < z_{max} \\ D_{B_{max}} \cdot \exp\left(-\frac{z - z_{max}}{z_d}\right), & z \geq z_{max} \end{cases} \quad (3)$$

Where z_{max} (m) is the depth down to which the maximum bioturbation coefficient ($D_{B_{max}}$) is applied, z_d (m) is the decaying length scale of $D_{B_{max}}$ ($m^2\ s^{-1}$).

D_M of dissolved matter in the pore water is a function of porosity, and is expressed as follows (Boudreau et al., 1998; Radtke et al., 2019):

$$D_M(z) = \frac{D^T}{1 - 2.02 \ln(\emptyset)} \quad (4)$$

where D^T ($m^2\ s^{-1}$) is the diffusion coefficient of the dissolved matter in the particle-free liquid at T ℃. The relationship between D^T and temperature (T) is expressed as (Soetaert et al., 1996):

$$D^T = D_0 + a \cdot T \quad (5)$$

where D_0 ($m^2\ s^{-1}$) is the diffusion coefficient of the dissolved matter in the particle-free liquid at 0 ℃, a ($m^2\ s^{-1}\ (℃)^{-1}$) is an ion-specific coefficient.

Bioirrigation characterizes the dissolved matter exchange caused by biological burrowing activities, and the coefficient decreases with depth (Dale et al., 2011):

$$\alpha(z) = \alpha_1 \cdot \frac{\exp(\alpha_2 - z)}{1 + \exp(\alpha_2 - z)} \quad (6)$$

The parameters α_1 (s^{-1}) and α_2 (m) represent the magnitude of bioirrigation and the depth at which it decreases to half of α_1, respectively.

The biochemical reactions are expressed in equations (7)-(12). Detailed descriptions of these reactions are presented in Table 1 (Soetaert et al., 1996; Capet et al., 2016; Akbarzadeh et al., 2018). These reaction equations primarily consider the limitations imposed by DO and temperature on each reaction. All the related coefficients and parameters are listed in Table 2. The sensitivity analysis of the model parameters is shown in Figure S3 and Text S1.

$$\sum R_{PON} = -R_{Min}^{OM} - R_{Den} - R_{Min}^{AM} - R_{DNRA} \quad (7)$$

$$\sum R_{NH_4^+} = R_{Min}^{OM} + R_{Den} + R_{Min}^{AM} - R_{Nit1} + (1 + 0.5 \cdot (1 - \delta) \cdot r_{C:N}) R_{DNRA} - R_{Ana} \quad (8)$$

$$\sum R_{NO_2^-} = 0.8 \cdot \alpha \cdot r_{C:N} \cdot R_{den} + R_{Nit1} - R_{Nit2} + 0.5 \cdot \delta \cdot r_{C:N} \cdot R_{DNRA} - R_{Ana} \quad (9)$$

$$\sum R_{NO_3^-} = R_{Nit2} - 0.8 \cdot r_{C:N} \cdot R_{den} - 0.5 \cdot r_{C:N} \cdot R_{DNRA} \quad (10)$$

$$\sum R_{O_2} = -r_{C:N} \cdot R_{Min}^{OM} - 1.5 \cdot R_{Nit1} - 0.5 \cdot R_{Nit2} - R_{ODUox} \quad (11)$$

$$\sum R_{ODU} = r_{C:N} \cdot (1 - r_{ODUsolid}) \cdot R_{Min}^{AM} - R_{ODUox} \quad (12)$$

215 Table 1. Reaction formulas and rate expressions.

Process	Formula	Rate expression
Oxic mineralization (R_{Min}^{OM})	$(CH_2O)_x(NH_3)_y + xO_2 \rightarrow yNH_4^+ + (x-y)CO_2 + yHCO_3^- + (x-y)H_2O$	$R_{Min}^{OM} = r_{min} \cdot PON \cdot Q^{\frac{T-20}{10}} \cdot \frac{O_2}{O_2 + Ks_{O_2}^{OM}} \cdot \frac{1}{\sum lim}$
Denitrification (R_{Den})	$(CH_2O)_x(NH_3)_y + 0.8xNO_3^- \rightarrow yNH_4^+ + 0.8\alpha xNO_2^- + 0.4(1-\alpha-\beta)xN_2 + 0.4\beta xN_2O + (0.2x - y + 0.8\alpha x)CO_2 + (0.8x - 0.8\alpha x + y)HCO_3^- + (0.6x - y - 0.8\alpha x - 0.4\beta x)H_2O + (0.8\alpha x - 0.4\beta x)H_2$	$R_{Den} = r_{min} \cdot PON \cdot Q^{\frac{T-20}{10}} \cdot \frac{NO_3^-}{NO_3^- + Ks_{NO_3^-}^{Den}} \cdot \frac{Kin_{O_2}^{Den}}{O_2 + Kin_{O_2}^{Den}} \cdot \frac{1}{\sum lim} \cdot \gamma$
Anoxic mineralization (R_{Min}^{AM})	$(CH_2O)_x(NH_3)_y + \text{an oxidant} \rightarrow yNH_4^+ + xCO_2 + xODU + xH_2O$	$R_{Min}^{AM} = r_{min} \cdot PON \cdot Q^{\frac{T-20}{10}} \cdot \frac{Kin_{O_2}^{AM}}{O_2 + Kin_{O_2}^{AM}} \cdot \frac{Kin_{NO_3^-}^{AM}}{NO_3^- + Kin_{NO_3^-}^{AM}} \cdot \frac{1}{\sum lim}$
Nitrification_step1 (R_{Nit1})	$NH_4^+ + 1.5O_2 + 2HCO_3^- \rightarrow NO_2^- + 3H_2O + 2CO_2$	$R_{Nit1} = r_{nit1} \cdot \frac{NH_4^+}{NH_4^+ + Ks_{NH_4^+}^{Nit1}} \cdot \frac{O_2}{O_2 + Ks_{O_2}^{Nit1}}$
Nitrification_step2 (R_{Nit2})	$NO_2^- + 0.5O_2 \rightarrow NO_3^-$	$R_{Nit2} = r_{nit2} \cdot \frac{NO_2^-}{NO_2^- + Ks_{NO_2^-}^{Nit2}} \cdot \frac{O_2}{O_2 + Ks_{O_2}^{Nit2}}$

DNRA (R_{DNRA})	$(CH_2O)_x(NH_3)_y + 0.5xNO_3^- + (1-\delta)xH^+ \rightarrow (0.5(1-\delta)x + y)NH_4^+ + 0.5\delta xNO_2^- + yHCO_3^- + (x-y)CO_2 + (0.5x - y - \delta x)H_2O + 1.5\delta xH_2$	$R_{DNRA} = r_{min} \cdot PON \cdot Q^{\frac{T-20}{10}} \cdot \frac{NO_3^-}{NO_3^- + Ks_{NO_3^-}^{Den}} \cdot \frac{Kin_{O_2}^{Den}}{O_2 + Kin_{O_2}^{Den}} \cdot \frac{1}{\sum lim} \cdot (1-\gamma)$
Anammox (R_{Ana})	$NH_4^+ + NO_2^- \rightarrow N_2 + 2H_2O$	$R_{Ana} = r_{Ana} \cdot \frac{NH_4^+}{NH_4^+ + Ks_{NH_4^+}^{Ana}} \cdot \frac{NO_2^-}{NO_2^- + Ks_{NO_2^-}^{Ana}} \cdot \frac{Kin_{O_2}^{Ana}}{O_2 + Kin_{O_2}^{Ana}}$
ODU oxidation (R_{ODUox})	$ODU + O_2 \rightarrow$ an oxidant	$R_{ODUox} = r_{ODUox} \cdot ODU \cdot \frac{O_2}{O_2 + Ks_{O_2}^{ODUox}}$

216 $\sum lim = \frac{O_2}{O_2+Ks_{O_2}^{OM}} + \frac{NO_3^-}{NO_3^-+Ks_{NO_3^-}^{Den}} \cdot \frac{Kin_{O_2}^{Den}}{O_2+Kin_{O_2}^{Den}} + \frac{Kin_{O_2}^{AM}}{O_2+Kin_{O_2}^{AM}} \cdot \frac{Kin_{NO_3^-}^{AM}}{NO_3^-+Kin_{NO_3^-}^{AM}}$. $x:y = C:N$.

217

Table 2. Model parameters. (L: based on literature; M: constrained with the model, I: independently determined from observations).

Parameter	Value	Unit	Description	References
ω	8.24×10^{-11}	m s^{-1}	Sedimentation velocity	L[a]
$D_{B_{max}}$	2×10^{-11}	m^2 s^{-1}	Maximum bioturbation coefficient	M
z_{max}	0.05	m	Depth down to which the maximum bioturbation coefficient is applied	L[b]
z_d	0.05	m	Decaying length scale of the maximum bioturbation coefficient	L[b, d]
$D_0^{NH_4^+}$	9.80×10^{-10}	m^2 s^{-1}	The molecular diffusion coefficient of NH_4^+ in a particle-free solution at 0 ℃	L[b]
$D_0^{NO_2^-}$	9.16×10^{-10}	m^2 s^{-1}	The molecular diffusion coefficient of NO_2^- in a particle-free solution at 0 ℃	L[c]
$D_0^{NO_3^-}$	9.78×10^{-10}	m^2 s^{-1}	The molecular diffusion coefficient of NO_3^- in a particle-free solution at 0 ℃	L[b]
D_0^{DO}	1.11×10^{-9}	m^2 s^{-1}	The molecular diffusion coefficient of DO (dissolved oxygen) in a particle-free solution at 0 ℃	L[b]
D_0^{ODU}	9.74×10^{-10}	m^2 s^{-1}	The molecular diffusion coefficient of ODU (the oxygen demand units) in a particle-free solution at 0 ℃	L[b]

$a_{NH_4^+}$	3.89×10^{-11}	$m^2\ s^{-1}\ (℃)^{-1}$	Coefficient for temperature dependency of diffusion coefficient of NH_4^+	L[b]
$a_{NO_2^-}$	3.89×10^{-11}	$m^2\ s^{-1}\ (℃)^{-1}$	Coefficient for temperature dependency of diffusion coefficient of NO_2^-	L[b]
$a_{NO_3^-}$	3.89×10^{-11}	$m^2\ s^{-1}\ (℃)^{-1}$	Coefficient for temperature dependency of diffusion coefficient of NO_3^-	L[b]
a_{DO}	4.47×10^{-11}	$m^2\ s^{-1}\ (℃)^{-1}$	Coefficient for temperature dependency of diffusion coefficient of DO	L[b]
a_{ODU}	2.80×10^{-11}	$m^2\ s^{-1}\ (℃)^{-1}$	Coefficient for temperature dependency of diffusion coefficient of ODU	L[b]
α_1	1.16×10^{-7}	s^{-1}	The magnitude of bioirrigation	M
α_2	0.09	m	the depth at which bioirrigation coefficient decreases to half of α_1	L[d]
r_{minf}	3×10^{-8}	s^{-1}	Mineralization coefficient of fast decay organic nitrogen	M
r_{mins}	7×10^{-10}	s^{-1}	Mineralization coefficient of slow decay organic nitrogen	M
Q	2		Factor for temperature effect on mineralization	L[e]
$Ks_{O_2}^{OM}$	3	$mmol\ m^{-3}$	Half saturation constant of DO in oxic mineralization	L[b]

$Ks_{NO_3^-}^{Den}$	30	mmol m^{-3}	Half saturation constant of NO_3^- in denitrification	L[b]
$Kin_{O_2}^{Den}$	10	mmol m^{-3}	Half saturation constant of DO in denitrification	L[b]
α	5	%	Nitrite leakage during denitrification	L[c]
β	1	%	Nitrous oxide leakage during denitrification	L[c]
γ	95	%	Fraction of total NO_3^- Reduction occurring via denitrification	L[c]
$Kin_{O_2}^{AM}$	5	mmol m^{-3}	Half saturation constant of DO in anoxic mineralization	L[b]
$Kin_{NO_3^-}^{AM}$	5	mmol m^{-3}	Half saturation constant of NO_3^- in anoxic mineralization	L[b]
r_{nit1}	1.16×10^{-4}	mmol m^{-3} s^{-1}	Maximum coefficient of nitrification (step 1)	M
r_{nit2}	1.16×10^{-3}	mmol m^{-3} s^{-1}	Maximum coefficient of nitrification (step 2)	M
$Ks_{NH_4^+}^{Nit1}$	10	mmol m^{-3}	Half saturation constant of NH_4^+ in nitrification (step 1)	L[c]
$Ks_{O_2}^{Nit1}$	15.6	mmol m^{-3}	Half saturation constant of DO in nitrification (step 1)	L[c]
$Ks_{NO_2^-}^{Nit2}$	10	mmol m^{-3}	Half saturation constant of NO_2^- in nitrification (step 2)	L[c]

$Ks_{O_2}^{Nit2}$	34.4	mmol m^{-3}	Half saturation constant of DO in nitrification (step 2)	L[c]
δ	5	%	Nitrite leakage during DNRA	L[c]
r_{Ana}	2.31×10^{-5}	mmol m^{-3} s^{-1}	Maximum anammox coefficient	M
$Ks_{NH_4^+}^{Ana}$	5	mmol m^{-3}	Half saturation constant of NH_4^+ in anammox	L[c]
$Ks_{NO_2^-}^{Ana}$	5	mmol m^{-3}	Half saturation constant of NO_2^- in anammox	L[c]
$Kin_{O_2}^{Ana}$	8	mmol m^{-3}	Half saturation constant of DO in anammox	L[c]
r_{ODUox}	1.16×10^{-5}	s^{-1}	Maximum ODU oxidation coefficient	L[f]
$Ks_{O_2}^{ODUox}$	1	mmol m^{-3}	Half saturation constant of DO in ODU oxidation	L[b]
$r_{ODUsolid}$	0.99	s^{-1}	Part of ODU production that is deposited as a solid	L[g]
$r_{C:N}$	10.2		Ratio of carbon to nitrogen	I
w	2.31×10^{-5}	m s^{-1}	Sinking velocity	L[h]
τ_c	0.06	N m^{-2}	Critical bottom stress	M
E_{PON}	1×10^{-8}	mmol m^{-2} s^{-1}	Resuspension coefficient	L[h]
D_{sur}	1×10^{-9}	m^2 s^{-1}	Surface diffusion coefficient	M
Δz	3×10^{-3}	m	Distance of the diffusion layer at sediment-water interface	L[i]

220 [a] Ichimi et al. (2005)

221 [b] Soetaert et al. (1996)

222 [c] Akbarzadeh et al. (2018)

223 [d] Dale et al. (2011)

224 [e] Capet et al. (2016)

225 [f] Laurent et al. (2016)

226 [g] Pastor et al. (2011)

227 [h] Ding et al. (2020)

228 [i] Wang et al. (2016)

229

Due to the large biomass of benthos and the characteristics of rapid change in the fluff layer, the mineralization coefficient in this layer is set to be 50 times faster than that in the sediment below it (Lee et al., 2002; Kuhrts et al., 2006; Laima et al., 2002).

At the sediment-water interface, the sinking and resuspension of PON depend on the bottom stress. The exchange flux (F_s) is expressed as (Wang, 2002):

$$F_s = \begin{cases} w \cdot C_s^w \cdot (\frac{\tau}{\tau_c} - 1), & \tau < \tau_c \\ E_s \cdot (\frac{\tau}{\tau_c} - 1), & \tau \geq \tau_c \end{cases} \quad (13)$$

where w ($m\,s^{-1}$) is the sinking velocity of particles in the bottom water, C_s^w ($mmol\,m^{-3}$) is concentration of PON in the bottom water, τ ($N\,m^{-2}$) is the bottom stress, τ_c ($N\,m^{-2}$) is the critical bottom stress, E_s ($mmol\,m^{-2}\,s^{-1}$) is the resuspension coefficient.

The exchanges of dissolved matters (NH_4^+, NO_2^-, NO_3^-, DO and ODU) are mainly through bioturbation, bioirrigation and molecular diffusion, and the flux (F_d) is expressed as (Boudreau et al., 1998):

$$F_d = -(D_{sur} + D_M^s) \cdot \emptyset \cdot \frac{C_d^w - C_d^{pw}}{\Delta z} \quad (14)$$

where D_{sur} ($m^2\,s^{-1}$) is the surface diffusion coefficient, D_M^s ($m^2\,s^{-1}$) is the surface molecular coefficient, C_d^{pw} ($mmol\,m^{-3}$) is the concentration of dissolved matter in the pore water of fluff layer, Δz (m) is the distance of the diffusion layer at sediment-water interface.

At the bottom of the model domain, the slow-decayed PON is allowed to move out as the burial process with a flux (B_s) as (Radtke et al., 2019):

$$B_s = \omega \cdot (1 - \emptyset) \cdot C_s^b \quad (15)$$

where superscript of b represents the deepest layer of the model domain.

The bottom fluxes (B_d) of NH_4^+, NO_2^- and ODU are expressed as:

$$B_d = -\left(D_B^b + D_M^b\right) \cdot \emptyset \cdot \frac{C_d^b - C_d^{bc}}{\Delta z^b} \quad (16)$$

where C_d^{bc} is NH_4^+ concentration in the pore water under the deepest layer of the model domain ($mmol\,m^{-3}$), whose values are given from observations.

2.4 Model configurations

Since this study focuses on seasonal changes at the sediment–water interface, the sediment depth in the model was set to 10 cm and uniformly divided into 100 layers.

The initial sediment concentration profile of PON was obtained from core observations in Harima Nada in July 2020, while those of NH_4^+, NO_2^- and NO_3^- were derived from observations conducted in April (Nakakuni et al., 2024). The DO profile was adopted from previous observations in the Seto Inland Sea (Sayama et al., 2002). The ODU concentration was initially set to 100 mmol m^{-3} and allowed to evolve dynamically within the model. In addition, the porosity profile was prescribed as a constant input condition throughout the simulation (Figure S4 and Text S2).

Monthly observations of bottom water temperature and concentrations of NH_4^+, NO_x^- ($NO_2^- + NO_3^-$) and DO from April 2020 to April 2021 were used to prescribe the upper boundary conditions, while NH_4^+ and NO_2^- concentration beneath the model domain from April 2020 to May 2021 served as the bottom boundary conditions (Nakakuni et al., 2024). The concentration of PON and NO_2^- in the bottom water were collected from the seasonal dataset of Japanese Ministry of the Environment from January 2020 to May 2021. The bottom stress was derived from a hydrodynamic model for the Seto Inland Sea (Zhu et al., 2019) (Figure 3). The ODU concentration in the bottom water was set to 0 mmol m^{-3}, while its concentration in the deeper sediment was assumed to be the initial value of 100 mmol m^{-3} (Soetaert et al., 1996). Forced by these boundary conditions, the sediment model simulated the nitrogen cycle changes in the sediments of Harima Nada from April 2020 to March 2021. And it was calculated for a long time (more than 170 years) to reach a steady-state condition, wherein the input and output fluxes of materials become balanced.

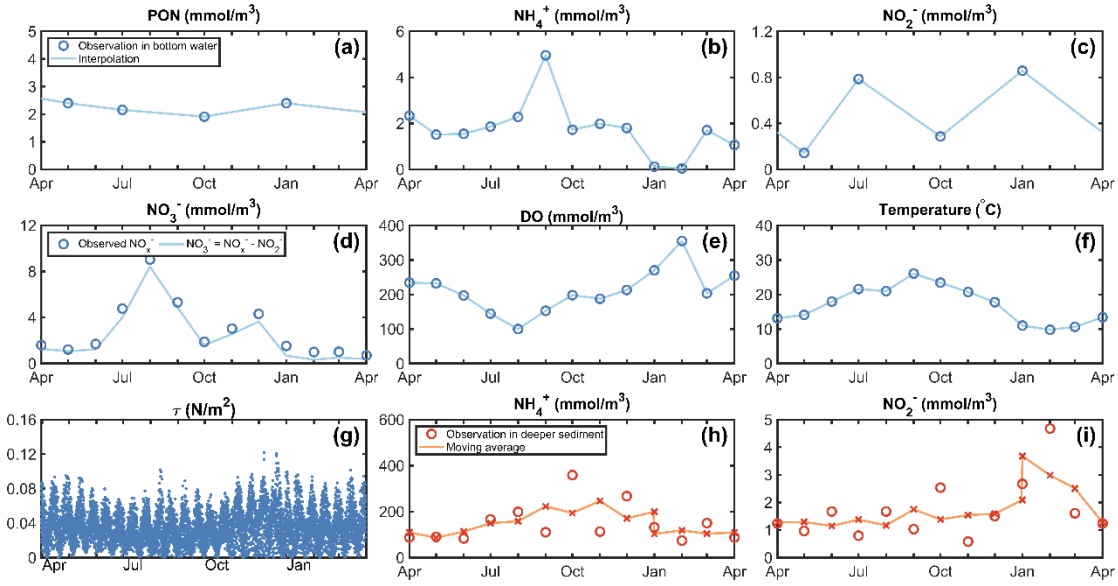

Figure 3. Model boundary conditions for the simulation period spanning April 2020 to March 2021: (a) PON concentration, (b) $\mathbf{NH_4^+}$ concentration, (c) $\mathbf{NO_2^-}$ concentration, (d) $\mathbf{NO_3^-}$ concentration, (e) DO concentration in the bottom water, (f) bottom water temperature, (g) bottom stress, (h) $\mathbf{NH_4^+}$ concentration and (c) $\mathbf{NO_2^-}$ concentration

in the layer below model domain (10-12 cm). The extrapolation shown in panels (a) and (c) utilizes the observed values from January 2020 and May 2021 for interpolation, which are not displayed in this figure. For panels (h) and (i), monthly observations are smoothed using a three-point moving average to reduce intra-seasonal variability.

3 Results

3.1 Seasonal variations of the particle and dissolved nitrogen concentrations in the sediment

The monthly concentrations of PON, NH_4^+, DO, NO_2^- and NO_3^- at different layers from 0 to 10 cm in the model domain are shown in Figure 4, alongside the corresponding observed data. The comparison between the model results and the observations, especially the seasonal variations, suggests a reliable performance of the model.

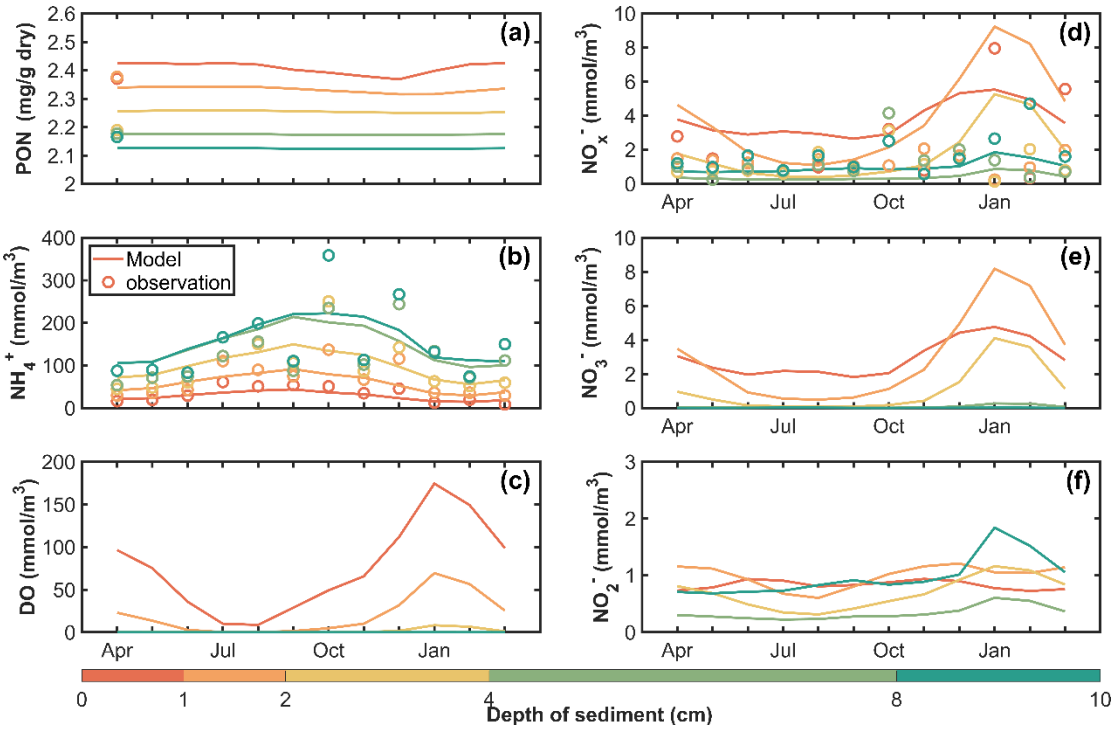

Figure 4. The seasonal variations of concentrations of (a) PON, (b) $\mathbf{NH_4^+}$, (c) DO, (d) $\mathbf{NO_x^-}$ $\mathbf{(NO_2^- + NO_3^-)}$, (e) $\mathbf{NO_3^-}$ and (f) $\mathbf{NO_2^-}$ in different layers in the sediment. Colours represent different depth. In all the panels, lines are model results and circles are the observation data.

The concentration of PON in the sediment was consistently greater in the surface layer compared to the underlying layers (Figure 4a). Its seasonal variation was apparent in the upper 2 cm of sediment and almost disappears in the layers below 2 cm. In the 0-1 cm layer, PON concentration decreased from a value of 2.43 mg/g in April to a minimum value of 2.37 mg/g in December, followed by an increase back

to 2.43 mg/g in March. In the deep layer of the sediment (8-10 cm), PON concentration remained around 2.12 mg/g throughout the year.

The NH_4^+ concentration had a minimum value at the surface and a maximum value at the deepest layer (Figure 4b), which was contrary to the vertical distribution of PON concentrations. The NH_4^+ concentrations presented significant seasonal variations across entire sediment layers, with the range of variation increasing with depth. For example, the NH_4^+ concentration in the 0-1 cm layer presented the lowest value of 14.65 mmol m^{-3} in February and the highest value of 43.79 mmol m^{-3} in September; however, the NH_4^+ concentration in the deep layer of the sediment (8-10 cm) presented the lowest value of 106.44 mmol m^{-3} in April and the highest value of 222.35 mmol m^{-3} in October. Except for the episodic high values observed in the deep sediment layer during autumn, the model successfully reproduced the seasonal variation of NH_4^+ concentration across all sediment layers, which was characterized by lower levels in winter and spring and elevated levels in summer and autumn.

The DO concentration profiles exhibited a clear vertical gradient, with higher values at the surface and lower values in deeper layers (Figure 4c). Surface DO reach a maximum of 174.51 mmol m^{-3} in January and decreased to a minimum of 8.70 mmol m^{-3} in August. The oxygen penetration depth (OPD) remained below 1 cm from June to October, and extended below 2 cm only during January and February.

NO_3^- was the dominant component of NO_x^- (Figure 4d, e). From December to April, a subsurface maximum appeared at the layer of 1–2 cm, whereas during the rest of the year the highest concentrations occurred at the surface layer. Within the 0–4 cm layer, NO_3^- exhibited a pronounced seasonal pattern, with lower concentrations in summer and higher concentrations in winter. Specifically, concentrations ranged from 1.82 to 4.76 mmol m^{-3} in the 0–1 cm layer, 0.49 to 8.18 mmol m^{-3} in the 1–2 cm layer, and 0.08 to 3.58 mmol m^{-3} in the 2–4 cm layer. Below 4 cm, NO_3^- concentrations remained close to zero throughout the year.

NO_2^- also showed the similar seasonal pattern, with lower concentrations in summer and higher concentrations in winter (Figure 4f). The maximum value of 1.84 mmol m^{-3} occurred in January at the deepest layer. Vertically, NO_2^- maxima alternated between the 0–2 cm layer and the 8–10 cm layer. Notably, during January to February, the maximum concentration in the 8–10 cm layer exceeded 1 mmol m^{-3}, whereas in other months the peak values remained around 1 mmol m^{-3}.

3.2 The flux of PON, DIN and N-loss (N_2 and N_2O) between bottom water and sediment

In this section, we introduce the flux at the sediment-water interface, including the net sinking of PON and the exchange of dissolved substances caused by molecular diffusion and bioturbation, excluding bioirrigation. PON sank from the bottom water to the sediment throughout the year (Figure 5a). The PON flux exhibited a bimodal seasonal pattern, with two peaks in July (2.14 mmol m^{-2} d^{-1}) and February (1.96 mmol m^{-2} d^{-1}), and a minimum in November (1.50 mmol m^{-2} d^{-1}).

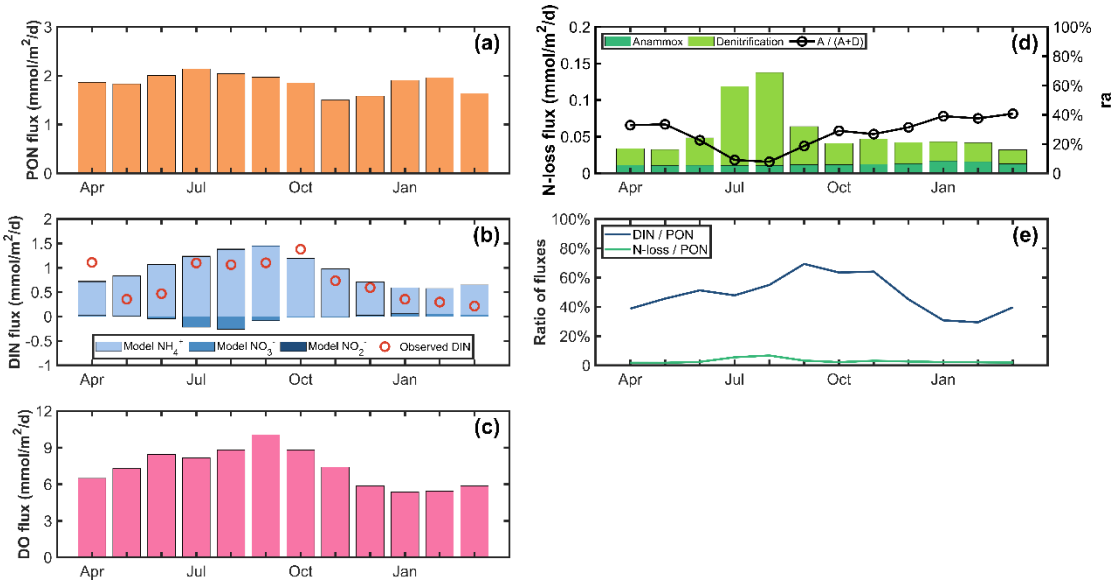

Figure 5. The fluxes of (a) PON, (b) DIN, (c) DO, (d) N-loss (N_2 and N_2O) at the sediment-water interface in the model, and (e) the ratios of DIN and N-loss fluxes to PON flux. The red circles in (b) are the values given by observations. DIN in (b) are sum of $\mathbf{NH_4^+}$, $\mathbf{NO_2^-}$ and $\mathbf{NO_3^-}$, whose fluxes are presented in different colour in the same panel.

DIN in the Harima Nada was released from the sediment into the bottom water throughout the year, exhibiting the highest flux of 1.37 mmol m^{-2} d^{-1} in September and the lowest flux of 0.58 mmol m^{-2} d^{-1} in February (Figure 5b). The DIN flux and its seasonal variation given by the model exhibit a general agreement with observations (Nakakuni et al., 2024). NH_4^+ flux dominated the seasonal variability of DIN flux, reaching a maximum of 1.44 mmol m^{-2} d^{-1} in September and a minimum of 0.52 mmol m^{-2} d^{-1} in February. In contrast, NO_3^- fluxes were substantially smaller. From June to November, NO_3^- was transported from the bottom water into the sediment, with a maximum influx of 0.26 mmol m^{-2} d^{-1} in August. From December to April, NO_3^- was released from the sediment into the overlying water, with a peak of 0.06 mmol m^{-2} d^{-1} in January. NO_2^- fluxes were negligible. A slight influx into the sediment occurred in January (0.002 mmol m^{-2} d^{-1}), whereas in all other months NO_2^- was released from the

sediment, with a maximum of 0.02 mmol m^{-2} d^{-1} in August. DO flux continuously supplies DO from the bottom water to the sediment and is the only source of DO for the sediment. It reached the highest value in September at 10.06 mmol m^{-2} d^{-1} and its lowest in January at 5.37 mmol m^{-2} d^{-1} (Figure 5c).

N-loss is produced through denitrification and anammox inside the sediment, which releases N_2 and N_2O to the atmosphere. N-loss flux across the sediment-water interface reached its peak of 0.14 mmol m^{-2} d^{-1} in August and the lowest value of 0.03 mmol m^{-2} d^{-1} in March (Figure 5d). Denitrification-derived N_2 and N_2O constituted the dominant components of N-loss flux and controlled its seasonal variability, with values ranging from 0.02 to 0.13 mmol m^{-2} d^{-1}. In contrast, N_2 production via anammox showed weak seasonal variation, remaining approximately constant at 0.01 mmol m^{-2} d^{-1}. Consequently, the relative contribution of anammox to N-loss flux (ra %) was lowest in August (8%) and highest in March (41%). Although N_2 was the main product of denitrification, the flux of N_2O, a potent greenhouse gas, was not negligible. It varied from 0.19 to 1.27 μmol m^{-2} d^{-1}, with a mean value of 0.44 μmol m^{-2} d^{-1}.

The ratio of DIN flux to PON flux ($R_{DIN/PON}$) reflects the fraction of nitrogen that sinks into the sediment and later releases back to the seawater (Figure 5e). $R_{DIN/PON}$ increased from 39% in April to a peak of 69% in September, with the annual average of 48%. The ratio of N-loss flux to PON flux ($R_{N\text{-}loss/PON}$) represented the proportion of nitrogen removed from the sediment. The highest value of $R_{N\text{-}loss/PON}$ was 7% in August while the lowest value was 2% in May. The sum of $R_{DIN/PON}$ and $R_{N\text{-}loss/PON}$ ranged from 32% in February to 73% in September, with an annual average of 51%. It suggested that around 50% of the PON flux sinking from seawater was retained in the sediment on average, with this retention rate potentially reaching nearly 70% during certain months.

3.3 The budgets of PON, NH_4^+ and NO_3^- in the sediment

The annual budgets for the four forms of nitrogen in the sediment of Harima Nada are estimated from the model results (Figure 6). The sinking of PON from bottom water was the source of PON in the sediment, quantified at 9.50 g N m^{-2} yr^{-1}. Since the primary production in the Harima Nada in 2020 was estimated to be 41 g N m^{-2} yr^{-1} (Tada, 2021), it could be interpreted that about 23% of the particles produced by primary production sank into the sediment. Within the deeper layers of the sediment, the burial rate of PON was 3.69 g N m^{-2} yr^{-1}, representing 39% of the PON flux into the sediment and 9% of

the primary production. The rest 5.74 g N m^{-2} yr^{-1} of PON flux into the sediment was mineralized to NH_4^+, which became the main source of NH_4^+ in the sediment.

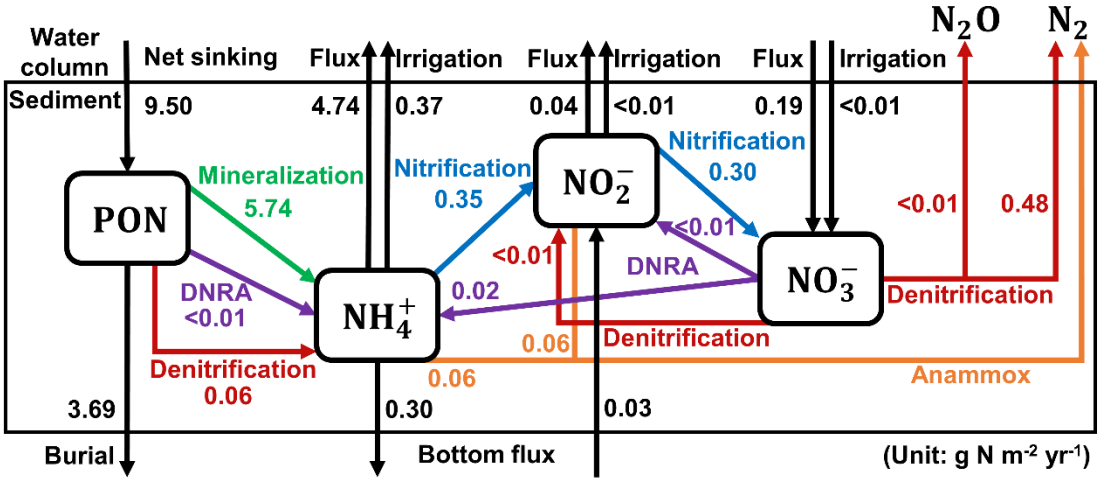

Figure 6. Nitrogen budgets in the sediment model of Harima Nada.

In addition to mineralization, NH_4^+ was also produced via denitrification and DNRA in the model, with the value of 0.06 g N m^{-2} yr^{-1} and 0.02 g N m^{-2} yr^{-1}, respectively. And 0.30 g N m^{-2} yr^{-1} of NH_4^+ was transferred to the deeper sediment located beneath the model domain. Furthermore, NH_4^+ has four sinks: the nitrification of NH_4^+ to NO_2^- had a rate of 0.35 g N m^{-2} yr^{-1}, the anammox of NH_4^+ to N_2 had a rate of 0.06 g N m^{-2} yr^{-1}, the upward NH_4^+ flux through the sediment-water interface was quantified at 4.74 g N m^{-2} yr^{-1} and 0.37 g N m^{-2} yr^{-1} of NH_4^+ was released from the sediment by bioirrigation.

At the sediment–water interface, NO_2^- was released into the overlying water with a flux of 0.04 g N m^{-2} yr^{-1}, while bioirrigation contributed less than 0.01 g N m^{-2} yr^{-1}. Nitrification converted 0.30 g N m^{-2} yr^{-1} of NO_2^- into NO_3^-. NO_3^- inputs from the bottom water to the sediment occurred via diffusive exchange and bioirrigation, amounting to 0.19 and less than 0.01 g N m^{-2} yr^{-1}, respectively. DNRA consumed 0.02 g N m^{-2} yr^{-1} of NO_3^-, whereas denitrification produced 0.48 g N m^{-2} yr^{-1} of N_2 and N_2O. In total, nitrogen removal processes (denitrification and anammox) generated 0.54 g N m^{-2} yr^{-1} of N_2 and N_2O, corresponding to approximately 6% of the PON sinking flux. Overall, bioirrigations are much weaker than fluxes in the exchange of solutes between sediments and water, and their seasonal variations shown in Figure S5 and Text S3.

4 Discussion

4.1 Factors affecting the seasonal variations of nitrogen inventories in the sediment

The model results show that the concentrations of PON, NH_4^+, NO_2^-, NO_3^- and DO in the sediment exhibit apparent seasonal variations. To clarify the factors controlling these seasonal variations, we carried out seven sensitivity experiments, in which we removed the seasonal variation of one of the following seven variables by substituting its monthly means with its annual mean: PON concentration (PON^{bw}), NH_4^+ concentration (NH_4^{+bw}), NO_3^- concentration (NO_3^{-bw}), NO_2^- concentration (NO_2^{-bw}), DO concentration (DO^{bw}), and water temperature in the overlying water, as well as bottom stress. Figure 7 shows the calculation results of the seven sensitivity experiments alongside the results described in Section 3 (referred to "Control" in Figure 7).

The concentration of PON^{bw}, bottom stress and the bottom water temperature significantly influence the seasonal variation of PON inventory in the sediment (Figure 7a). Sinking of PON^{bw} serves as the source of PON in the sediment, controlled by the concentration of PON^{bw} and bottom stress. The variations in bottom water temperature can change the mineralization rate in the sediment (Figure S6a and Text S4). Although these seasonal variations can directly impact the PON inventory, the extent of seasonal variation in PON inventory is relatively minor, with its value being more than two orders of magnitude smaller than the overall PON inventory.

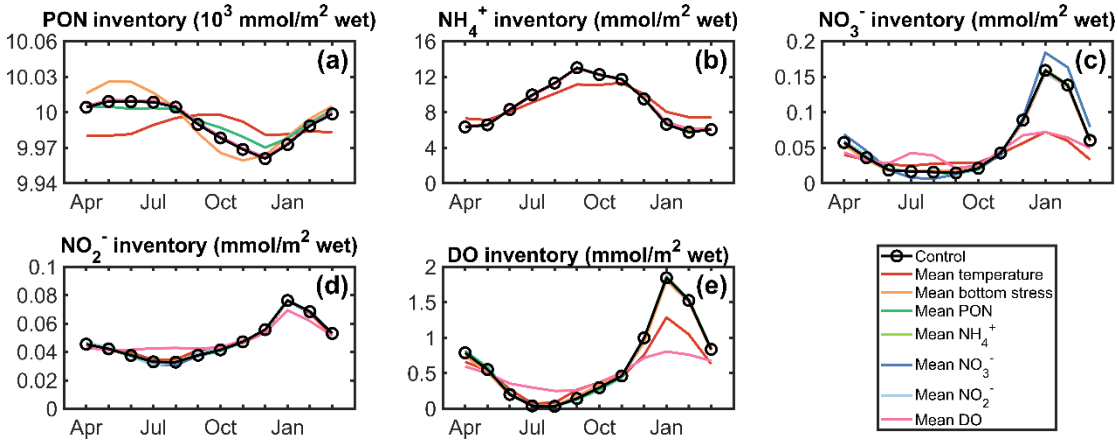

Figure 7. Comparisons of the model results among eight calculations (seven sensitivity experiments and one control run). The sensitivity experiments include the cases removing the seasonal variations of PON concentration (dark green line, "Mean PON"), $\mathbf{NH_4^+}$ concentration (light green line, "Mean $\mathbf{NH_4^+}$"), $\mathbf{NO_3^-}$ concentration (dark blue line, "Mean $\mathbf{NO_3^-}$"), $\mathbf{NO_2^-}$ concentration (light blue line, "Mean $\mathbf{NO_2^-}$"), DO concentration (pink line, "Mean DO") and water temperature (red line, "Mean temperature") in the overlying water, as well as of the bottom stress (orange line, "Mean bottom stress"). (a) PON inventory; (b) $\mathbf{NH_4^+}$ inventory; (c) $\mathbf{NO_3^-}$ inventory; (d) $\mathbf{NO_2^-}$ inventory; (e) DO inventory.

Among the 7 factors, only the bottom water temperature is responsible for the seasonal variations of NH_4^+ inventory (Figure 7b) as it affects the mineralization rate that produces NH_4^+ in the sediment (Figure S6 and Text S4). NH_4^+ is produced primarily through mineralization and is predominantly released to the overlying water. Due to the very low NH_4^{+bw} concentration (Figure 3b) and the relatively minor contributions of other biogeochemical processes compared to mineralization (Figure 6), bottom water temperature serves as the primary environmental factor regulating NH_4^+ inventory.

NO_3^- inventory is mainly controlled by bottom water temperature, DO^{bw}, and NO_3^{-bw} concentration (Figure 7c). High temperatures in summer enhance denitrification (Figure S6d), leading to substantial NO_3^- consumption. At the same time, low DO^{bw} concentrations limit DO supply to the sediment, thereby suppressing nitrification and further reducing NO_3^- availability (Figure S6b, c). Consequently, NO_3^- concentrations are relatively low in summer. In contrast, during winter, NO_3^- is better preserved in the sediment, resulting in higher concentrations. However, the lower NO_3^{-bw} concentration during winter also constrains its supply to the sediment. As an intermediate product of nitrification, NO_2^- is primarily controlled by DO^{bw} concentration (Figure 7d).

Since sedimentary DO is supplied exclusively from the overlying water, DO concentrations within the sediment are largely governed by DO^{bw} (Figure 7e). In winter, lower temperatures reduce the consumption of DO through mineralization, allowing more DO to be preserved within the sediment. This also explains the deeper OPD occurred in winter.

4.2 Factors affecting the seasonal variations in the sediment-water fluxes of nitrogen

The seasonal variation in concentration of PON^{bw} and the bottom stress are the main factors deciding the seasonal variation of PON flux across the interface between the bottom water and sediment (Figure 8a). High concentration of PON^{bw} increases the sinking flux of PON from seawater to sediment. An inverse seasonal relationship can be discerned between PON flux and bottom stress (Figure 3h). The rise in bottom stress during the spring and winter induces the resuspension of PON at the sediment-water interface, thereby diminishing the downward PON flux.

The bottom water temperature controls not only the seasonal variations of NH_4^+ inventory in the sediment (Figure 7b) but also that of NH_4^+ flux from the sediment to the bottom water (Figure 8b). This

is because NH_4^+ concentration in the sediment is much higher than the concentration of NH_4^{+bw}, and its variation directly determines the change of NH_4^+ flux (Figure 3b and Figure 4b).

Bottom water temperature, DO^{bw}, and NO_3^{-bw} concentration jointly drive the summer peak of NO_3^- flux into the sediment (Figure 8c). On the one hand, high temperatures in summer enhance mineralization, increasing NH_4^+ production and thereby supplying substrate for nitrification. On the other hand, high temperatures accelerate molecular diffusion, strengthening solute exchange across the sediment–water interface. However, the low DO concentration in the sediment during summer suppress nitrification, while relatively low sedimentary NO_3^- concentrations favor the flux of NO_3^- from the bottom water into the sediment. In addition, the relatively high NO_3^{-bw} concentration during summer further contributes to the enhanced downward NO_3^- flux. NO_2^- flux is comparatively small and exhibit high sensitivity to variations in bottom water temperature, as well as NO_3^{-bw}, NO_2^{-bw}, and DO^{bw} concentrations (Figure 8d).

The DO flux is primarily controlled by bottom water temperature (Figure 8e). Temperature regulates molecular diffusion and thus governs the exchange of DO across the sediment–water interface. Furthermore, the low DO^{bw} concentrations associated with the formation of the summer bottom cold water in Harima Nada also play a key role in limiting DO flux.

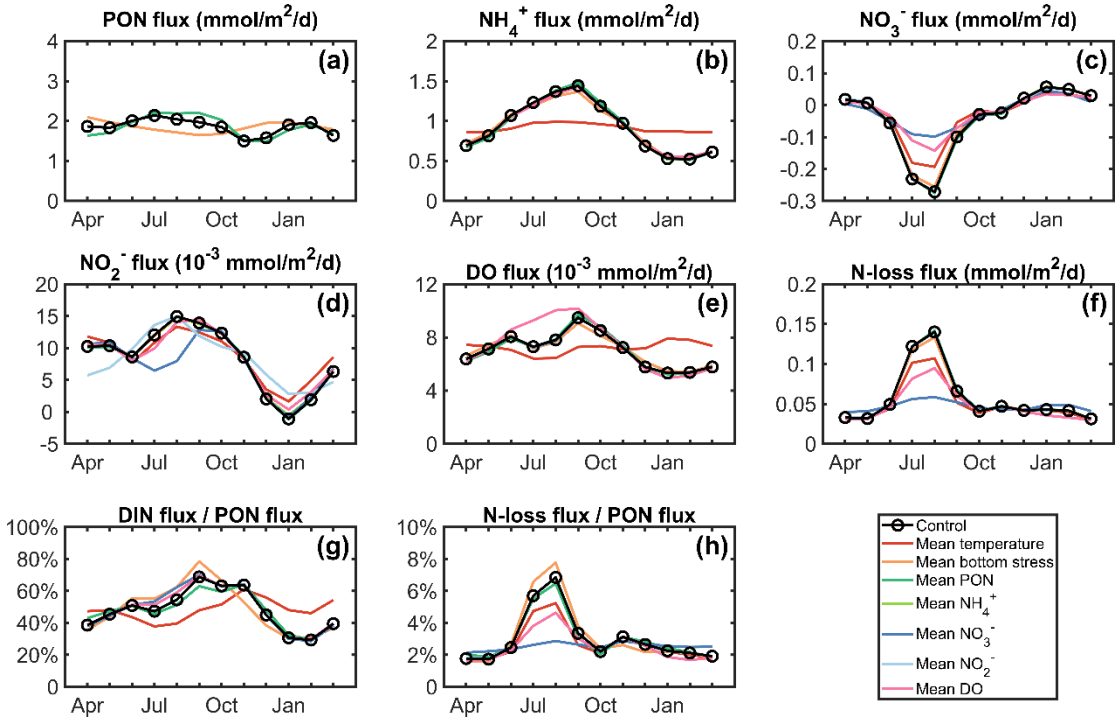

Figure 8. Comparisons of the model results among eight calculations (seven sensitivity experiments and one control run). The sensitivity experiments include the cases removing the seasonal variations of PON concentration (dark

462 green line, "Mean PON"), $\mathbf{NH_4^+}$ concentration (light green line, "Mean $\mathbf{NH_4^+}$"), $\mathbf{NO_3^-}$ concentration (dark blue line,
463 "Mean $\mathbf{NO_3^-}$"), $\mathbf{NO_2^-}$ concentration (light blue line, "Mean $\mathbf{NO_2^-}$"), DO concentration (pink line, "Mean DO") and
464 water temperature (red line, "Mean temperature") in the overlying water, as well as of the bottom stress (orange line,
465 "Mean bottom stress"). (a) PON flux; (b) $\mathbf{NH_4^+}$ flux; (c) $\mathbf{NO_3^-}$ flux; (d) $\mathbf{NO_2^-}$ flux; (e) DO flux; (f) N-loss flux; (g)
466 ratio of DIN flux to PON flux; (h) ratio of N-loss to PON flux.

467 The differences in the factors controlling the seasonal variation of PON and DIN fluxes indicate that a
468 large PON flux into the sediment does not necessarily lead to a corresponding increase in DIN flux from
469 the sediment to the bottom water. This suggests that estimating the DIN flux by using reflective boundary
470 conditions based only on the concentration of PON^{bw}, or relying on empirical formulations that neglect
471 bottom water temperature, may lead to considerable errors in the representing of the seasonal variation
472 in DIN flux.

473 The N-loss flux is dominated by denitrification (Figure 6). However, the NO_3^- concentration in summer
474 sediments is low and needs to be supplemented by NO_3^{-bw}. This results in NO_3^- flux contributing to the
475 summer peak of denitrification. Therefore, its seasonal variability of N-loss flux is controlled by factors
476 similar to those governing NO_3^- flux (Figure 8f). $R_{DIN/PON}$ and $R_{N\text{-}loss/PON}$ are two important parameters
477 for comprehending the nitrogen cycle in the semi-enclosed inland sea. The seasonal variation of $R_{DIN/PON}$
478 is likely controlled by bottom water temperature and bottom stress (Figure 8g), while that of $R_{N\text{-}loss/PON}$
479 is affected by bottom water temperature, DO^{bw}, and NO_3^{-bw} concentration (Figure 8h).

480 **4.3 Comparisons with other coastal seas**

481 Numerous studies have evaluated the nitrogen fluxes at the sediment-water interface, yielding varying
482 conclusions (Zhou et al., 2017; Sun et al., 2021; Canion et al., 2014; Lin et al., 2017; De Vittor et al.,
483 2012; Mu et al., 2017; Rich et al., 2020; Dale et al., 2022; Bohlen et al., 2011; Ratmaya et al., 2022;
484 Zhou et al., 2022). In this subsection, we compare the fluxes of NH_4^+, NO_3^- and N-loss calculated by our
485 sediment model with the values reported in these studies for different coastal seas (Table 3).
486

Table 3. Benthic fluxes (mmol m^{-2} d^{-1}) reported in some regions; positive values represent the release from sediment to water.

Flux	Value		Location	References
NH_4^+	1.53	to 1.62	Northern Adriatic Sea	(De Vittor et al., 2012)
	0.16	to 1.39	Mauritanian upwelling region	(Dale et al., 2022)
	0.12	to 5.3	Vilaine Bay	(Ratmaya et al., 2022)
	-0.1077	to 0.219	Areas off eastern Taiwan	(Zhou et al., 2017)
	-0.71	to 0.14	Bohai Bay	(Mu et al., 2017)
	-0.1	to 0.066	Yellow Sea and East China Sea	(Zhou et al., 2022)
	0	to 4	Peruvian upwelling region	(Bohlen et al., 2011)
	0.0867	to 0.4722	Taranto Gulf	(De Vittor et al., 2015)
	0.52	to 1.44	Harima Nada	This study
NO_3^-	-0.46	to -0.26	Northern Adriatic Sea	(De Vittor et al., 2012)
	-3	to -0.1	Mauritanian upwelling region	(Dale et al., 2022)
	-0.62	to 0.46	Vilaine Bay	(Ratmaya et al., 2022)
	-0.241	to 0.00005	Areas off eastern Taiwan	(Zhou et al., 2017)
	1.43	to 2.26	Bohai Bay	(Mu et al., 2017)
	-3.43	to 0.082	Yellow Sea and East China Sea	(Zhou et al., 2022)
	-3.8	to -0.3	Peruvian upwelling region	(Bohlen et al., 2011)
	4.8	to 8.8	Taranto Gulf	(De Vittor et al., 2015)
	-0.26	to 0.06	Harima Nada	This study
N_2	2.7	to 544.3	Chinese marginal seas	(Sun et al., 2021)

28.70	to 420.49	East China Sea	(Lin et al., 2017)
0.2	to 2.8	Arctic shelf	(Canion et al., 2014)
1322.4	to 2683.2	Peru margin	(Rich et al., 2020)
0.03	to 0.14	Harima Nada	This study

489

490 NH_4^+ is released from the sediment to the bottom water in our study area. Such upward flux has been
491 commonly observed in other coastal regions, including Northern Adriatic Sea (De Vittor et al., 2012),
492 Vilaine Bay (Ratmaya et al., 2022) and Eastern Taiwan (Zhou et al., 2017).
493 NO_3^- flux exhibits pronounced seasonal variability in both magnitude and direction. In Harima Nada, the
494 formation of strong stratification in summer promotes the appearance of hypoxic conditions and limits
495 the supply of DO to the sediment. As a result, nitrification is suppressed and cannot effectively replenish
496 sedimentary NO_3^-. Meanwhile, the seasonal peak in bottom water NO_3^- concentration promotes the
497 transport of NO_3^- from the water column into the sediment. Although the seasonal reversal in flux
498 direction differs from that reported for Vilaine Bay, the underlying controlling mechanisms are similar
499 (Ratmaya et al., 2022). Therefore, the seasonal variations in temperature and bottom water NO_3^-
500 concentration jointly regulate the magnitude and direction of nitrate flux. In contrast, in areas such as the
501 offshore of eastern Taiwan, the sediment continuously absorbs NO_3^- from the overlying water because
502 of the lower concentration of NO_3^- in the pore water compared to the overlying water (Zhou et al., 2017).
503 The N-loss flux is an important sink of nitrogen in the sediment of the Harima Nada, constituting about
504 6% of the sinking flux of PON into the sediment. The flux of N_2 estimated in our study is about one to
505 two orders of magnitude smaller than the values reported in other areas such as the East China Sea and
506 Arctic shelf. This discrepancy may be attributed to higher bacterial activity in those areas or to elevated
507 concentrations of organic matter and NO_3^- in the sediment (Sun et al., 2021; Canion et al., 2014; Lin et
508 al., 2017; Rich et al., 2020). Our results indicate that denitrification is the dominant pathway contributing
509 to nitrogen removal, consistent with numerous previous studies (Teng and Lin, 2024; Dalsgaard et al.,
510 2005). In the sediment, NO_2^-, as an intermediate, remains at relatively low concentrations and is
511 insufficient to sustain high rates of anammox. Consequently, the availability of NO_2^- primarily governs
512 the seasonal variability of the relative contribution of anammox to N-loss flux. In particular, summer
513 hypoxia leads to low NO_2^- production, which suppresses anammox while favoring denitrification,
514 resulting in the lowest relative contribution of anammox during this period.
515

5 Conclusions

This study developed a one-dimensional vertical sediment model to investigate the seasonal variations in the direction and magnitude of nitrogen fluxes at the sediment-water interface in semi-enclosed inland seas, and to reveal the controlling mechanisms of various environmental factors on these variations. Utilizing continuous observational data from a typical semi-enclosed inland sea for validation, we found that the flux of PON settling from the bottom water to the sediment is the main source of nitrogen in the sediment, with its seasonal variation governed by the PON concentration in the bottom water and bottom stress. Due to the regeneration of a substantial amount of NH_4^+ in the sediment, NH_4^+ is continuously released from the sediment to the overlying water, with its seasonal variation controlled by bottom water temperature. Temperature influences the mineralization rate, which subsequently affects NH_4^+ flux through NH_4^+ inventory in the sediment. Under the combined control of bottom water temperature and NO_3^- concentration, both the direction and magnitude of NO_3^- flux exhibited significant seasonal variations. This results in the seasonal variation of DIN flux returning from the sediment to the water being unrelated to the PON flux, as they are controlled by different environmental factors with distinct seasonal patterns. This finding suggests that neglecting to consider bottom water temperature and nitrogen concentrations in reflective boundary conditions or empirical formulas may lead to varying degrees of misestimation when calculating the seasonal variation of DIN flux at the sediment-water interface.

Denitrification is the main process of the nitrogen removal and contributes to the seasonal variation of N-loss. However, the overall nitrogen removal amount is relatively low, possibly due to the low NO_3^- concentration in the bottom water caused by the oligotrophic environment of Harima Nada. In addition, this model is mainly suited for semi-enclosed inland seas dominated by muddy sediments and does not account for the advection of pore water flow in sandy sediments. In practice, this process can be incorporated by adjusting the vertical velocity in the solute transport equation. Overall, this model can be widely applied to investigate nitrogen cycling-related issues in nearshore muddy sediments. Moreover, by investigating the seasonal variations of nitrogen cycling in semi-enclosed inland sea sediments and their controlling factors, it can provide a basis for governance and management support for environmental issues such as coastal eutrophication.

In future research, we will expand upon this study by integrating it with long-term observational data to investigate the effects of prolonged changes in aquatic environments, such as eutrophication and seawater warming, on sediment nitrogen cycling and nitrogen flux at the sediment-water interface.

Code, data, or code and data availability

The source code of the numerical model used in this study is available on request. Please contact the corresponding author.

Author contributions

Zhaosen Wu: conceptualization, methodology, software, validation, visualization, writing (original draft preparation). Xinyu Guo: formal analysis, methodology, resources, supervision, writing (review and editing). Jie Shi: supervision, writing (review and editing). Xiaokun Ding: methodology, software. Masatoshi Nakakuni: data curation, investigation, resources. Kuninao Tada: data curation, investigation, resources.

Competing interests

The authors declare that they have no conflict of interest.

Supporting Information

Supporting Information is available free of charge at the Biogeosciences website.

Acknowledgement

This research was performed by the Environment Research and Technology Development Fund (JPMEERF20255002) of the Environmental Restoration and Conservation Agency Provided by the Ministry of Environment of Japan. We thank Dr. Akihiko Morimoto and Dr. Naoki Yoshie who worked in the Center for Marine Environmental Studies, Ehime University, Japan and provided valuable suggestions for our research. Z. Wu thanks the China Scholarship Council (CSC) and the Ministry of Education, Culture, Sports, Science and Technology, Japan (MEXT) for a project on Joint Usage/Research Center, Leading Academia in Marine and Environmental Research (LaMer) for supporting his study in Japan.

References

Akbarzadeh, Z., Laverman, A. M., Rezanezhad, F., Raimonet, M., Viollier, E., Shafei, B., and Van Cappellen, P.: Benthic nitrite exchanges in the Seine River (France): An early diagenetic modeling analysis, Sci Total Environ, 628-629, 580-593, 10.1016/j.scitotenv.2018.01.319, 2018.

Berelson, W. M., McManus, J., Severmann, S., and Reimers, C. E.: Benthic flux of oxygen and nutrients across Oregon/California shelf sediments, Cont. Shelf Res., 55, 66-75, 10.1016/j.csr.2013.01.009, 2013.

Berner, R.: Early diagenesis: a theoretical approach: Princeton, 1980.

Bohlen, L., Dale, A. W., Sommer, S., Mosch, T., Hensen, C., Noffke, A., Scholz, F., and Wallmann, K.: Benthic nitrogen cycling traversing the Peruvian oxygen minimum zone, Geochim. Cosmochim. Acta, 75, 6094-6111, 10.1016/j.gca.2011.08.010, 2011.

Boudreau, B. P., Mucci, A., Sundby, B., Luther, G. W., and Silverberg, N.: Comparative diagenesis at three sites on the Canadian continental margin, J. Mar. Res., 56, 1259-1284, 10.1357/002224098765093634, 1998.

Boynton, W. R., Ceballos, M. A. C., Bailey, E. M., Hodgkins, C. L. S., Humphrey, J. L., and Testa, J. M.: Oxygen and Nutrient Exchanges at the Sediment-Water Interface: a Global Synthesis and Critique of Estuarine and Coastal Data, Estuaries Coasts, 41, 301-333, 10.1007/s12237-017-0275-5, 2017.

Canion, A., Overholt, W. A., Kostka, J. E., Huettel, M., Lavik, G., and Kuypers, M. M.: Temperature response of denitrification and anaerobic ammonium oxidation rates and microbial community structure in Arctic fjord sediments, Environ Microbiol, 16, 3331-3344, 10.1111/1462-2920.12593, 2014.

Capet, A., Meysman, F. J. R., Akoumianaki, I., Soetaert, K., and Grégoire, M.: Integrating sediment biogeochemistry into 3D oceanic models: A study of benthic-pelagic coupling in the Black Sea, Ocean Modelling, 101, 83-100, 10.1016/j.ocemod.2016.03.006, 2016.

Chang, P.-H., Guo, X., and Takeoka, H.: A numerical study of the seasonal circulation in the Seto Inland Sea, Japan, Journal of Oceanography, 65, 721-736, 10.1007/s10872-009-0062-4, 2009.

Chen, S., Gao, D., Zhang, J., Zheng, Y., Li, X., Dong, H., Yin, G., Han, P., Liang, X., Liu, M., Müller, C., and Hou, L.: Gross nitrogen transformations in intertidal sediments of the Yangtze Estuary: Distribution patterns and environmental controls, Geoderma, 429, 10.1016/j.geoderma.2022.116233, 2023.

Dale, A. W., Clemens, D., Dähnke, K., Korth, F., Wankel, S. D., Schroller-Lomnitz, U., Wallmann, K., and Sommer, S.: Nitrogen cycling in sediments on the NW African margin inferred from N and O isotopes in benthic chambers, Frontiers in Marine Science, 9, 10.3389/fmars.2022.902062, 2022.

Dale, A. W., Sommer, S., Bohlen, L., Treude, T., Bertics, V. J., Bange, H. W., Pfannkuche, O., Schorp, T., Mattsdotter, M., and Wallmann, K.: Rates and regulation of nitrogen cycling in seasonally hypoxic sediments during winter (Boknis Eck, SW Baltic Sea): Sensitivity to environmental variables, Estuar. Coast. Shelf Sci., 95, 14-28, 10.1016/j.ecss.2011.05.016, 2011.

Dalsgaard, T., Thamdrup, B., and Canfield, D. E.: Anaerobic ammonium oxidation (anammox) in the marine environment, Research in microbiology, 156, 457-464, 2005.

De Vittor, C., Relitti, F., Kralj, M., Covelli, S., and Emili, A.: Oxygen, carbon, and nutrient exchanges at the sediment–water interface in the Mar Piccolo of Taranto (Ionian Sea, southern Italy), Environmental Science and Pollution Research, 23, 12566-12581, 10.1007/s11356-015-4999-0, 2015.

De Vittor, C., Faganeli, J., Emili, A., Covelli, S., Predonzani, S., and Acquavita, A.: Benthic fluxes of oxygen, carbon and nutrients in the Marano and Grado Lagoon (northern Adriatic Sea, Italy), Estuarine, Coastal and Shelf Science, 113, 57-70, 10.1016/j.ecss.2012.03.031, 2012.

Devol, A. H.: Denitrification, Anammox, and N2 Production in Marine Sediments, Annu. Rev. Mar. Sci., 7, 403-423, 10.1146/annurev-marine-010213-135040, 2015.

Ding, X., Guo, X., Zhang, C., Yao, X., Liu, S., Shi, J., Luo, C., Yu, X., Yu, Y., and Gao, H.: Water conservancy project on the Yellow River modifies the seasonal variation of Chlorophyll-a in the Bohai Sea, Chemosphere, 254, 126846, 10.1016/j.chemosphere.2020.126846, 2020.

Han, A., Kao, S. J., Lin, W., Lin, Q., Han, L., Zou, W., Tan, E., Lai, Y., Ding, G., and Lin, H.: Nutrient Budget and Biogeochemical Dynamics in Sansha Bay, China: A Coastal Bay Affected by Intensive Mariculture, Journal of Geophysical Research: Biogeosciences, 126, 10.1029/2020jg006220, 2021.

Huang, F., Lin, X., Hu, W., Zeng, F., He, L., and Yin, K.: Nitrogen cycling processes in sediments of the Pearl River Estuary: Spatial variations, controlling factors, and environmental implications, CATENA, 206, 105545, https://doi.org/10.1016/j.catena.2021.105545, 2021.

Huettel, M., Berg, P., and Kostka, J. E.: Benthic Exchange and Biogeochemical Cycling in Permeable Sediments, Annu. Rev. Mar. Sci., 6, 23-51, 10.1146/annurev-marine-051413-012706, 2014.

631 Ichimi, K., Tada, K., and Montani, S.: The phytoplankton assemblage of the past and present in the Seto
632 Inland Sea-the expectation from sediment core samples, Aquabiology, 27, 214～221, 2005.
633 Ishii, D., Yanagi, T., and Sasakura, S.: Long-term trends in the occurrence of red tides in the Seto Inland
634 Sea, Japan, Oceanography in Japan, 23, 217-236, 10.5928/kaiyou.23.6_217, 2014.
635 Jäntti, H. and Hietanen, S.: The Effects of Hypoxia on Sediment Nitrogen Cycling in the Baltic Sea,
636 Ambio, 41, 161-169, 10.1007/s13280-011-0233-6, 2012.
637 Kalvelage, T., Lavik, G., Lam, P., Contreras, S., Arteaga, L., Löscher, C. R., Oschlies, A., Paulmier, A.,
638 Stramma, L., and Kuypers, M. M. M.: Nitrogen cycling driven by organic matter export in the South
639 Pacific oxygen minimum zone, Nature Geoscience, 6, 228-234, 10.1038/ngeo1739, 2013.
640 Khalil, M. A. K. and Rasmussen, R. A.: The global sources of nitrous oxide, Journal of Geophysical
641 Research: Atmospheres, 97, 14651-14660, 10.1029/92jd01222, 2012.
642 Kuhrts, C., Seifert, T., and Fennel, W.: Modeling Transport of Fluff Layer Material in the Baltic Sea,
643 Hydrobiologia, 554, 25-30, 10.1007/s10750-005-1003-x, 2006.
644 Laima, M., Maksymowska-Brossard, D., Sauriau, P.-G., Richard, P., Girard, M., Gouleau, D., and
645 Joassard, L.: Fluff deposition on intertidal sediments: effects on benthic biota, ammonium fluxes and
646 nitrification rates, Biogeochemistry, 61, 115-133, 10.1023/a:1020264414924, 2002.
647 Laurent, A., Fennel, K., Wilson, R., Lehrter, J., and Devereux, R.: Parameterization of biogeochemical
648 sediment–water fluxes using in situ measurements and a diagenetic model, Biogeosciences, 13, 77-94,
649 10.5194/bg-13-77-2016, 2016.
650 Lee, J.-Y., Tett, P., Jones, K., Jones, S., Luyten, P., Smith, C., and Wild-Allen, K.: The PROWQM
651 physical–biological model with benthic–pelagic coupling applied to the northern North Sea, J. Sea Res.,
652 48, 287-331, https://doi.org/10.1016/S1385-1101(02)00182-X, 2002.
653 Leng, Q., Guo, X., Zhu, J., and Morimoto, A.: Contribution of the open ocean to the nutrient and
654 phytoplankton inventory in a semi-enclosed coastal sea, Biogeosciences, 20, 4323-4338, 10.5194/bg-20-
655 4323-2023, 2023.
656 Leynaert, A., Longphuirt, S. N., An, S., Lim, J.-H., Claquin, P., Grall, J., Kwon, B. O., and Koh, C. H.:
657 Tidal variability in benthic silicic acid fluxes and microphytobenthos uptake in intertidal sediment,
658 Estuarine, Coastal and Shelf Science, 95, 59-66, 10.1016/j.ecss.2011.08.005, 2011.

Lin, X., Liu, M., Hou, L., Gao, D., Li, X., Lu, K., and Gao, J.: Nitrogen Losses in Sediments of the East China Sea: Spatiotemporal Variations, Controlling Factors, and Environmental Implications, Journal of Geophysical Research: Biogeosciences, 122, 2699-2715, 10.1002/2017jg004036, 2017.

Liu, H. and Yin, B.: Annual cycle of carbon, nitrogen and phosphorus in the Bohai Sea: A model study, Cont. Shelf Res., 27, 1399-1407, 10.1016/j.csr.2007.01.015, 2007.

Liu, S. M., Li, L. W., Zhang, G. L., Liu, Z., Yu, Z., and Ren, J. L.: Impacts of human activities on nutrient transports in the Huanghe (Yellow River) estuary, Journal of Hydrology, 430-431, 103-110, 10.1016/j.jhydrol.2012.02.005, 2012.

Liu, X., Stock, C. A., Dunne, J. P., Lee, M., Shevliakova, E., Malyshev, S., and Milly, P. C. D.: Simulated Global Coastal Ecosystem Responses to a Half-Century Increase in River Nitrogen Loads, Geophysical Research Letters, 48, e2021GL094367, https://doi.org/10.1029/2021GL094367, 2021.

Lønborg, C. and Markager, S.: Nitrogen in the Baltic Sea: Long-term trends, a budget and decadal time lags in responses to declining inputs, Estuarine, Coastal and Shelf Science, 261, 107529, https://doi.org/10.1016/j.ecss.2021.107529, 2021.

McTigue, N. D., Gardner, W. S., Dunton, K. H., and Hardison, A. K.: Biotic and abiotic controls on co-occurring nitrogen cycling processes in shallow Arctic shelf sediments, Nature Communications, 7, 13145, 10.1038/ncomms13145, 2016.

Mei Liu, S., Wei Li, L., and Zhang, Z.: Inventory of nutrients in the Bohai, Cont. Shelf Res., 31, 1790-1797, 10.1016/j.csr.2011.08.004, 2011.

Mu, D., Yuan, D., Feng, H., Xing, F., Teo, F. Y., and Li, S.: Nutrient fluxes across sediment-water interface in Bohai Bay Coastal Zone, China, Mar. Pollut. Bull., 114, 705-714, 10.1016/j.marpolbul.2016.10.056, 2017.

Nakakuni, M., Yamaguchi, H., Ichimi, K., and Tada, K.: Seasonal variation in pore water nutrients and their fluxes from the bottom sediments in Harima Nada, Seto Inland Sea, Journal of Oceanography, 80, 219-232, 10.1007/s10872-024-00719-7, 2024.

Niemistö, J., Kononets, M., Ekeroth, N., Tallberg, P., Tengberg, A., and Hall, P. O. J.: Benthic fluxes of oxygen and inorganic nutrients in the archipelago of Gulf of Finland, Baltic Sea – Effects of sediment resuspension measured in situ, J. Sea Res., 135, 95-106, 10.1016/j.seares.2018.02.006, 2018.

687 Pastor, L., Cathalot, C., Deflandre, B., Viollier, E., Soetaert, K., Meysman, F. J. R., Ulses, C., Metzger,
688 E., and Rabouille, C.: Modeling biogeochemical processes in sediments from the Rhône River prodelta
689 area (NW Mediterranean Sea), Biogeosciences, 8, 1351-1366, 10.5194/bg-8-1351-2011, 2011.
690 Radtke, H., Lipka, M., Bunke, D., Morys, C., Woelfel, J., Cahill, B., Böttcher, M. E., Forster, S., Leipe,
691 T., Rehder, G., and Neumann, T.: Ecological ReGional Ocean Model with vertically resolved sediments
692 (ERGOM SED 1.0): coupling benthic and pelagic biogeochemistry of the south-western Baltic Sea,
693 Geoscientific Model Development, 12, 275-320, 10.5194/gmd-12-275-2019, 2019.
694 Ratmaya, W., Laverman, A. M., Rabouille, C., Akbarzadeh, Z., Andrieux-Loyer, F., Barillé, L., Barillé,
695 A.-L., Le Merrer, Y., and Souchu, P.: Temporal and spatial variations in benthic nitrogen cycling in a
696 temperate macro-tidal coastal ecosystem: Observation and modeling, Cont. Shelf Res., 235,
697 10.1016/j.csr.2022.104649, 2022.
698 Rich, J. J., Arevalo, P., Chang, B. X., Devol, A. H., and Ward, B. B.: Anaerobic ammonium oxidation
699 (anammox) and denitrification in Peru margin sediments, J. Mar. Syst., 207,
700 10.1016/j.jmarsys.2018.09.007, 2020.
701 Sayama, M., Sohma, A., and Takasugi, Y.: Experimental analysis of the effect of flow velocity on oxygen
702 dynamics near the water-sediment interface in a coastal zone., Proceedings of Coastal Engineering, 49,
703 996-1000, 10.2208/proce1989.49.996, 2002.
704 Soetaert, K., Herman, P. M. J., and Middelburg, J. J.: A model of early diagenetic processes from the
705 shelf to abyssal depths, Geochim. Cosmochim. Acta, 60, 1019-1040, 10.1016/0016-7037(96)00013-0,
706 1996.
707 Sun, L., Wang, C., Yu, H., Liu, D., Houlton, B. Z., Wang, S., Zeng, X., Bai, E., Fang, Y., and Jia, Y.:
708 Biotic and Abiotic Controls on Dinitrogen Production in Coastal Sediments, Glob. Biogeochem. Cycle,
709 35, 10.1029/2021gb007069, 2021.
710 Tada, K.: Primary Production, Nutrients and Nutrient Release from Bottom Sediments in Coastal Water,
711 Journal of Water Environment Society of Japan, 44, 137-141, 2021.
712 Teng, Z. and Lin, X.: Sediment nitrates reduction processes affected by non-native Sonneratia apetala
713 plantation in South China, Sci. Total Environ., 906, 167523, 2024.
714 Thamdrup, B.: New Pathways and Processes in the Global Nitrogen Cycle, Annual Review of Ecology,
715 Evolution, and Systematics, 43, 407-428, 10.1146/annurev-ecolsys-102710-145048, 2012.

716 Tong-u-dom, S., Morimoto, A., Leng, Q., and Guo, X.: Seasonal variation in the current field and
717 development of bottom cold water in Harima-Nada, Journal of Oceanography, 80, 1-20, 10.1007/s10872-
718 023-00702-8, 2023.
719 Tong-U-Dom, S., Morimoto, A., Guo, X., Leng, Q., Yoshie, N., Tada, K., Ichimi, K., Yamaguchi, H.,
720 and Nakakuni, M.: Lower trophic ecosystem dynamics in the eastern part of the Seto Inland Sea and their
721 response to changes in nutrient supply from the rivers, Prog. Oceanogr., 239,
722 10.1016/j.pocean.2025.103565, 2025.
723 Umlauf, L., Klingbeil, K., Radtke, H., Schwefel, R., Bruggeman, J., and Holtermann, P.: Hydrodynamic
724 Control of Sediment-Water Fluxes: Consistent Parameterization and Impact in Coupled Benthic-Pelagic
725 Models, Journal of Geophysical Research: Oceans, 128, 10.1029/2023jc019651, 2023.
726 Wang, J., Zhao, L., Fan, R., and Wei, H.: Scaling relationships for diffusive boundary layer thickness
727 and diffusive flux based on in situ measurements in coastal seas, Prog. Oceanogr., 144, 1-14,
728 10.1016/j.pocean.2016.03.001, 2016.
729 Wang, X. H.: Tide-Induced Sediment Resuspension and the Bottom Boundary Layer in an Idealized
730 Estuary with a Muddy Bed, Journal of Physical Oceanography, 32, 3113-3131, 10.1175/1520-
731 0485(2002)032<3113:Tisrat>2.0.Co;2, 2002.
732 Wilson, S. T., Al-Haj, A. N., Bourbonnais, A., Frey, C., Fulweiler, R. W., Kessler, J. D., Marchant, H.
733 K., Milucka, J., Ray, N. E., Suntharalingam, P., Thornton, B. F., Upstill-Goddard, R. C., Weber, T. S.,
734 Arévalo-Martínez, D. L., Bange, H. W., Benway, H. M., Bianchi, D., Borges, A. V., Chang, B. X., Crill,
735 P. M., del Valle, D. A., Farías, L., Joye, S. B., Kock, A., Labidi, J., Manning, C. C., Pohlman, J. W.,
736 Rehder, G., Sparrow, K. J., Tortell, P. D., Treude, T., Valentine, D. L., Ward, B. B., Yang, S., and
737 Yurganov, L. N.: Ideas and perspectives: A strategic assessment of methane and nitrous oxide
738 measurements in the marine environment, Biogeosciences, 17, 5809-5828, 10.5194/bg-17-5809-2020,
739 2020.
740 Yamamoto, T., Orimoto, K., Asaoka, S., Yamamoto, H., and Onodera, S.-i.: A Conflict between the
741 Legacy of Eutrophication and Cultural Oligotrophication in Hiroshima Bay, Oceans, 2, 546-565,
742 10.3390/oceans2030031, 2021.

Yang, J.-Y. T., Hsu, T.-C., Tan, E., Lee, K., Krom, M. D., Kang, S., Dai, M., Hsiao, S. S.-Y., Yan, X., and Zou, W.: Sedimentary processes dominate nitrous oxide production and emission in the hypoxic zone off the Changjiang River estuary, Sci. Total Environ., 827, 154042, 2022.

Yi, Y., Gao, Y., Wu, X., Jia, W., and Liu, Q.: Modeling the effect of artificial flow and sediment flux on the environment and plankton of an estuary, International Journal of Sediment Research, 38, 335-348, https://doi.org/10.1016/j.ijsrc.2023.02.001, 2023.

Zhang, X., Ward, B. B., and Sigman, D. M.: Global Nitrogen Cycle: Critical Enzymes, Organisms, and Processes for Nitrogen Budgets and Dynamics, Chem Rev, 120, 5308-5351, 10.1021/acs.chemrev.9b00613, 2020.

Zhang, X., Zhang, Q., Yang, A., Hou, L., Zheng, Y., Zhai, W., and Gong, J.: Incorporation of microbial functional traits in biogeochemistry models provides better estimations of benthic denitrification and anammox rates in coastal oceans, Journal of Geophysical Research: Biogeosciences, 123, 3331-3352, 2018.

Zhou, F., Gao, X., Zhang, Y., Yuan, H., Song, J., Liu, K., Yang, B., and Zhuang, W.: Potential mobility of inorganic nutrients and its controls at the sediment-water interface in the main path of Kuroshio Current off eastern Taiwan, Mar Pollut Bull, 119, 270-276, 10.1016/j.marpolbul.2017.04.002, 2017.

Zhou, N., Zhang, G. L., and Liu, S. M.: Nutrient exchanges at the sediment-water interface and the responses to environmental changes in the Yellow Sea and East China Sea, Mar Pollut Bull, 176, 113420, 10.1016/j.marpolbul.2022.113420, 2022.

Zhu, J., Guo, X., Shi, J., and Gao, H.: Dilution characteristics of riverine input contaminants in the Seto Inland Sea, Mar. Pollut. Bull., 141, 91-103, 10.1016/j.marpolbul.2019.02.029, 2019.